Int. J. Electrochem. Sci., 12 **(2017)** 11987 – 11996, doi: 10.20964/2017.12.28

International Journal of
ELECTROCHEMICAL
SCIENCE
www.electrochemsci.org

Short Communication

Preparation of TiO_2/Co_3O_4 Nanostructured Materials by a Two-Step Hydrothermal Method and their Electrode Performance in Lithium Ion Batteries

Ju Rong[1,2,3], *Meng Kun*[2], *Xiaohua Yu*[2,*], *Zhang Yannan*[2,*]

[1] Institute of Metal Research, Chinese Academy of Sciences, Shenyang 110016, China.
[2] National Engineering Research Center of solid waste resource, Kunming University of Science and Technology, Kunming 650093, China.
[3] University of Chinese Academy of Sciences, Beijing 100049, China
[*]E-mail: xiaohua_y@163.com, zyn_legolas@163.com

Received: 26 June 2017 / *Accepted:* 9 August 2017 / *Published:* 12 November 2017

In order to increase the cycling performance and reversible capacity of Co_3O_4 electrode materials, TiO_2/Co_3O_4 anode materials were prepared by a two-step hydrothermal method. The phase composition, structure and morphology of the TiO_2/Co_3O_4 anode materials were characterized by X-ray diffraction, scanning electron microscopy and transmission electron microscopy. The electrode performance of the materials was tested by a battery discharge and charge tester and an electrochemical workstation. The results shows that the TiO_2/Co_3O_4 nanostructured materials consist of a new type of nest-like nanostructure, formed by an external mechanical force. A single nest-like TiO_2/Co_3O_4 nanostructure is composed of the monoclinic TiO_2-B and cubic Co_3O_4 phases. The nanostructured materials have excellent electrochemical performance, with a capacity of 650 mAh/g and a current density of 33.5 mA/g after 100 cycles.

Keywords: TiO_2/Co_3O_4; lithium batteries; anode material; nanostructured

1. INTRODUCTION

In recent decades, with the huge consumption of oil, coal and other traditional energy sources, and increasingly severe environmental pollution, green renewable energy has become a hot topic in global research [1]. Secondary lithium-ion batteries are considered as ideal energy conversion and storage devices, but their commercial requirements in terms of energy and power density are ever increasing [2,3].

The anode is an important part of the lithium-ion battery and its performance is essential to the overall device [4]. At present, the academic community generally believes that TiO_2 is a high performance anode material and that it has good application prospects in the field of lithium-ion batteries because it has high rate capability, stable cycling performance, fast charge and discharge performance and large specific capacity [5–7]. For example, the theoretical specific capacity of the polymorphic substance TiO_2(B) is 335 mAh/g.

In addition, the theoretical specific capacity of Co_3O_4 is up to 890 mAh/g, twice that of ordinary commercial graphite electrodes, meaning that it has also become a popular research topic in recent years [8–10]. Many nanostructures of Co_3O_4, such as nanowires, nanoneedles and nanosheets, are superior to other materials, such as Si, Sn and SnO_2, in terms of specific capacity and cycling performance [11–15]. However, studies have found that the current challenge for Co_3O_4 is that the capacity loss is great after the end of charge and discharge, resulting in poor cycling performance. Therefore, how to improve the cycling performance of Co_3O_4 and improve its reversible capacity are key scientific problems in the lithium-ion battery community.

Based on the advantages of TiO_2 and Co_3O_4, this work proposes an approach to prepare TiO_2/Co_3O_4 nanostructured materials by a two-step hydrothermal method, under the action of an external mechanical force field. The microstructures, phase composition and electrode performance of the TiO_2/Co_3O_4 anode materials were analyzed by XRD, SEM, TEM, a battery discharge and charge tester and an electrochemical workstation.

2. EXPERIMENTAL

2.1. Synthesis

Table 1 shows the specifications of the reagents and the manufacturers. The TiO_2 nanowires can be prepared as follows: i) prepare 30 mL of NaOH solution with a concentration of 10 mol/L and mix it evenly with 0.2 g of TiO_2 nanopowder; ii) pour it into a 100 mL reaction still and have it react in a heat collected thermostatic heating magnetic stirrer (DF-101S) at a reaction temperature of 130 °C for 24 h; iii) after the reaction is complete, use deionized water to wash the precipitate separated out to a pH value of 9; iv) use the 0.2 mol/L dilute nitric acid to wash it to a pH value of ~7.

After completing the preparation of the TiO_2 nanowires: i) place the TiO_2 nanowires in 60 mL of deionized water together with 4.5 g of cobalt nitrate hexahydrate and 4.5 g of urea, and conduct electromagnetic stirring for 1 h; ii) carry out the second hydrothermal reaction by placing the well stirred solution in a 100 mL reaction still and put it in an oven to have it react at a temperature of 180 °C for 12 h; iii) after the reaction still is cooled down naturally, cleanse the solution with anhydrous ethanol and deionized water, respectively; iv) dry it in a tube furnace, under an argon shield, at 400 °C for 5 h.

After completing the preparation of the TiO_2/Co_3O_4 nanostructured materials; i) mix the TiO_2/Co_3O_4 nanostructured materials, acetylene black and polyvinylidene fluoride at a mass ratio of 7:2:1; ii) stir them well into a slurry with the appropriate amount of *N*-methylpyrrolidone as the solvent

and apply the slurry onto the copper foil to produce negative plates; iii) use Celgard-2400 microporous polypropylene as the membrane and 1 mol/L $LiPF_6$/ethyl carbonate + dimethyl carbonate + ethyl methyl carbonate (at a volume ratio of 1:1:1, respectively) as the electrolyte; iv) assembly them into a CR2025 button battery in a glove box filled with argon.

Table 1. Specifications of the reagents and the manufacturers.

Name	Specifications and purity	Consumption	Manufacturers
NaOH	99.99% AR	10 mol/L×0.03 L	Shanghai Aladdin Inc.
P25 TiO_2	99.99% AR	0.2 g	AEROSIL200
Urea	99.00% AR	4.5 g	Shanghai Aladdin Inc.
$Co_3O_4 \cdot H_2O$	99.00% AR	4.5 g	Shanghai Aladdin Inc.

2.2. Material characterization

The phase structures of the materials were tested using XRD (D/MAX-2200). The structure, morphology and element distributions of the materials were characterized by FE-SEM (FEI-QUANTA200) and TEM (FEI Tecnia G2F30 S-TWIN).

2.3. Electrochemical measurement

At an ambient temperature, a battery test system (CT-3008) was used to test the charge and discharge and cycling performances of the samples at a voltage range of 0–3 V and at a current density of 33.5 mA/g. An electrochemical workstation (CHI660E) was used to test the cyclic voltammetry curve, with the scanning voltage of 0–3 V, scanning rate of 2 mV/s and the prepared button battery does not undergo the charge-discharge treatment. The electrochemical workstation (CHI660E) was also used to analyze the electrochemical impedance of the samples. The test was carried out at room temperature, the working electrode was the electrode material prepared for the experiment and the auxiliary and reference electrodes were metal lithium plates.

3. RESULTS AND DISCUSSION

3.1. Surface appearance analysis on the structure of TiO_2/Co_3O_4

The structural properties of a composite material have a significant effect on the intercalation and de-intercalation of lithium ions [16]. It is generally considered that the greater the specific surface area, the better the lithium performance [17,18]. Fig. 1 shows the FE-SEM images of the TiO_2 nanowires (1a) and TiO_2/Co_3O_4 composites (1b), respectively. In Fig. 1b, the upper right part is the partial enlarged view. In Fig. 1a, the TiO_2 nanowires gather together as bundles, with a large draw

ratio, which are nanowires with a certain growth orientation and uniform distribution, and a single nanowire is ~20 μm long. In Fig. 1b, the TiO_2/Co_3O_4 composite material possesses a nest-like structure, where there is no obvious agglomeration, indicating that the material has good dispersion. In order to further observe the appearance of the TiO_2/Co_3O_4 composite structure, we selected one of the feature points for observation. It can be seen from the partial enlargement diagram that the nest-like TiO_2/Co_3O_4 is composed of multiple flake and linear structures supporting each other, which can greatly improve the structural stability. The size of a single nest-like TiO_2/Co_3O_4 structure is ~20 μm, indicating that the specific surface area is large. In summary, nest-like TiO_2/Co_3O_4 nanostructures are prepared through a secondary hydrothermal reaction. In this structure, the size of a nest cell is ~20 μm and the flake and linear structures forming the nest are ~20 μm long and 50 nm wide.

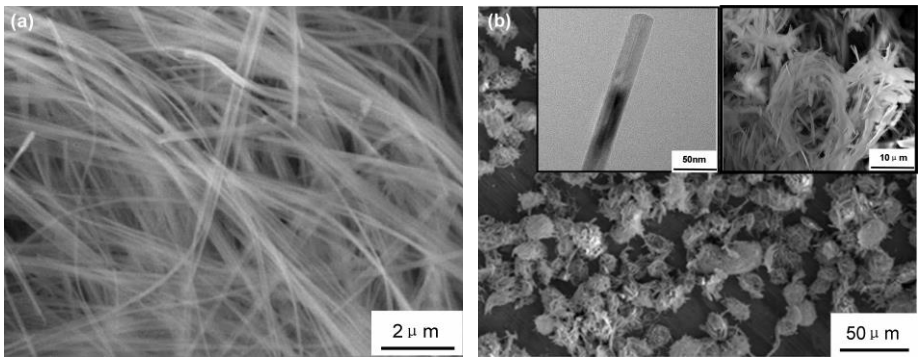

Figure 1. FE-SEM images of (a) TiO_2 nanowires (at 180 °C for 12 h) and (b) TiO_2/Co_3O_4 nanostructures (at 180 °C for 12 h under the argon shield, with sintering at 400 °C for 5 h).

Fig. 2a shows the TEM diagram of the nest-like TiO_2/Co_3O_4 nanostructure, which is consistent with that in Fig. 1b. In order to clarify the distribution of elements, we conducted EDS spectrum analysis on the flaky part a_1 and the linear part a_2 in Fig. 2a, respectively. The results are shown in Figs. 2b and c, respectively. It can be seen that the flake structure is mainly composed of Co and the linear structure is mainly composed of Ti.

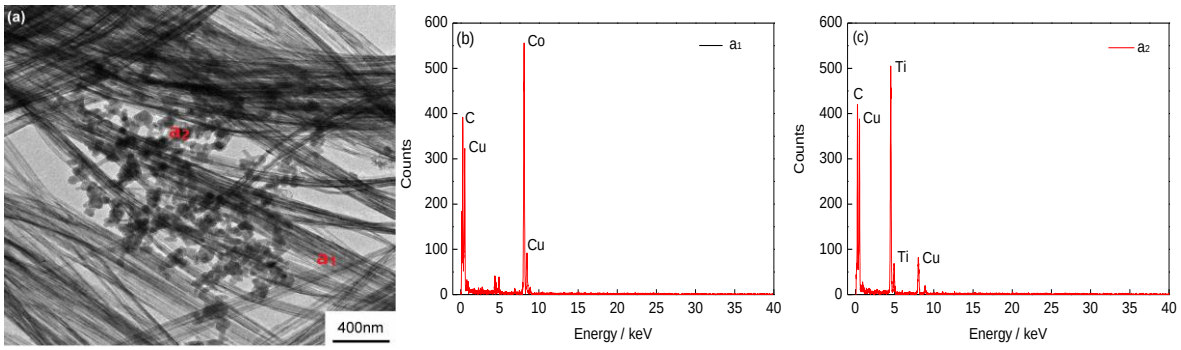

Figure 2. TEM and EDS patterns of TiO_2/Co_3O_4 nanostructure.

3.2. Analysis on the phase composition of the nest-like TiO_2/Co_3O_4 nanostructure

In order to further study the elemental composition and phase distribution of the composite structure, the nest-like TiO_2/Co_3O_4 nanostructured materials were tested and analyzed using XRD. Fig. 3 shows the XRD patterns of the TiO_2 nanowires and nest-like TiO_2/Co_3O_4 nanostructured materials. From the patterns of the TiO_2 nanowires, we can see that there are several obvious diffraction peaks in the range of 2θ = 10°–80°, and there is no obvious impurity peak. The peak position is mostly consistent with that of the monoclinic TiO_2-B (JCPDS No.74-1940), but there are some smaller diffraction peaks that match those of anatase, which is because, with increasing temperature, TiO_2-B is formed into the anatase phase during the annealing process [19,20]. In the nest-like TiO_2/Co_3O_4 nanostructure map, it can be seen that the diffraction peaks of Co_3O_4 are consistent with those in the standard map of the cubic-phase Co_3O_4 (JCPDS No.74-2120). The diffraction peaks are sharp and the crystal is complete, and compared with the XRD pattern of TiO_2, the diffraction peaks are obviously narrowed, indicating that the crystallinity of the composite structure is good. However, at the same time, there are also diffraction peaks of CoO, which means that the reaction is not complete during the annealing process. In summary, the nest-like TiO_2/Co_3O_4 nanostructure is composed of monoclinic TiO_2-B and cubic-phase Co_3O_4.

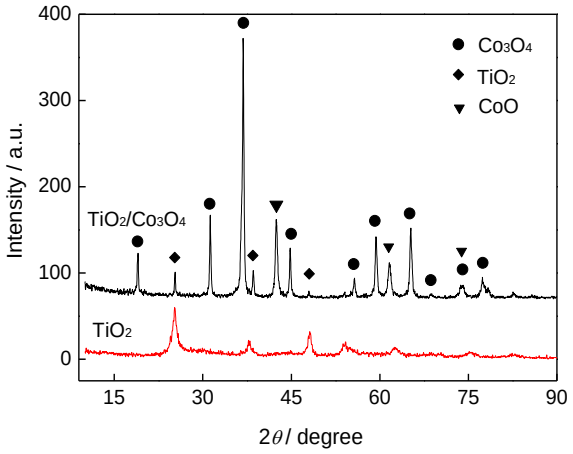

Figure 3. XRD patterns of TiO_2 nanowires and TiO_2/Co_3O_4 nanostructures.

3.3. Electrochemical performance analysis

3.3.1. Constant current charge-discharge test

Fig. 4 shows the constant current charge-discharge curves of the TiO_2 nanowires, Co_3O_4 nanosheets and nest-like TiO_2/Co_3O_4 nanostructures. It can be seen that during the first discharge of the TiO_2 electrode, the voltage quickly falls from the initial value down to ~2 V, and then remains flat at 1.7 V for a very short time, before finally falling to the cut-off voltage. In the first charge, the voltage also remains flat at ~1.25 V for a very short period (Fig. 4a). The electrode exhibits a high initial reversible charge–discharge capacity, with a first discharge capacity of 295 mAh/g and a first

charge capacity of 285 mAh/g, indicating that the irreversible capacity is only 10 mAh/g. In the subsequent cycle, the material discharge capacity is stabilized at ~261 mAh/g, indicating good stability [21–23].

The Co_3O_4 nanosheet structure has a discharge capacity of 1666 mAh/g and a charge capacity of 884 mAh/g during the first charge-discharge cycle, meaning that the irreversible capacity is up to 782 mAh/g and that the Coulombic efficiency is only 53% (Fig. 4b). The high irreversible capacity is caused by the formation of an SEI film and the electrolyte decomposition in the charge and discharge process. Alternatively [24,25], it may arise from damage to the structure caused by the intercalation and de-intercalation of lithium ions in the charge and discharge cycle due to the unstable flake structure [26,27]. In the subsequent cycles, the discharge capacity of the Co_3O_4 nanosheet structure is continuously attenuated, with the second discharge capacity at 824 mAh/g and the third discharge capacity reduced to 597 mAh/g. In the fifth cycle, the discharge capacity is only 427 mAh/g.

The TiO_2/Co_3O_4 nest-like nanostructure remains stable when the voltage drops to 1.5 V during the first discharge, and it has a long discharge plateau at 0.75 V. The voltage then continues to drop rapidly to 0 V. The initial discharge capacity of the material is 777 mAh/g, and the charge capacity is 759 mAh/g, meaning that the irreversible capacity is 18 mAh/g. The first charge and discharge capacity is higher than 295 mAh/g of TiO_2 in Fig. 4a, and the irreversible capacity is slightly increased, which is presumed to be caused by the formation of the SEI film during the first discharge. In the first five cycles, the capacity decreases slowly and finally stabilizes at ~720 mAh/g. In the subsequent cycles, the charge and discharge curves coincide well, which fully shows that starting from the first charge process, the battery charge–discharge reversibility is improved.

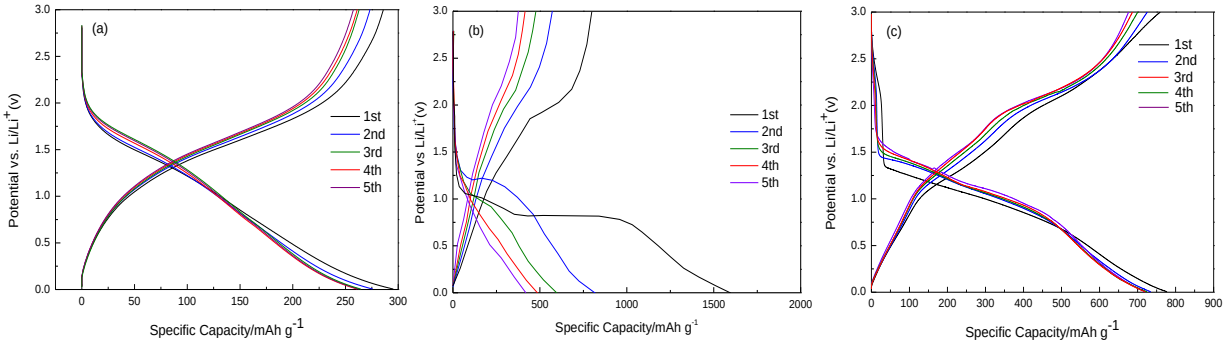

Figure 4. Charge-discharge curves of (a) TiO_2 nanowires (at 180 ℃ for 12 h), (b) Co_3O_4 nanosheets and (c) TiO_2/Co_3O_4 nanostructures (at 180 ℃ for 12 h under the argon shield, with sintering at 400 ℃ for 5 h) at a voltage ranging between 0 and 3 V and a current density of 33.5 mA/g.

3.3.2. Cycling performance test

Fig. 5 shows the cycling performance curve of the nest-like TiO_2/Co_3O_4 nanostructures at a current density of 0.1 C and within a test voltage range of 0–3 V after being cycled for 100 times. It can be seen that the discharge capacity of the nest-like TiO_2/Co_3O_4 nanostructure can reach ~650 mAh/g after 100 cycles, and during the 100 cycles, the discharge capacity remains basically stable,

indicating that the nest-like TiO_2/Co_3O_4 nanostructures have excellent cycling performance. After 100 cycles, the structure can still maintain a high reversible capacity and capacity retention rate.

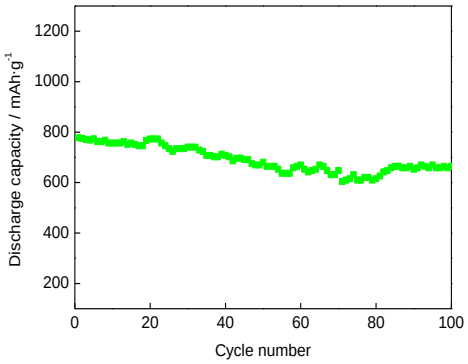

Figure 5. Discharge capacity and cycling performance curve of TiO_2/Co_3O_4 nanostructures.

Fig. 6 shows the rate capability test diagram of the nest-like TiO_2/Co_3O_4 nanostructures. During the test, the current density is 0.1, 0.2, 0.5 and 1 C, respectively. The structure is fully charged and discharged five times at each current density and finally charged and discharged five times at the low current density of 0.1 C. It can be seen from Fig. 6 that as the current density increases, the capacity of the ultra-fine ultra-long TiO_2-B nanowire electrode decreases gradually. The overall change remains steady, except a large capacity loss between 0.5 and 1 C, which is ~125 mAh/g, probably due to the unstable binding of TiO_2 nanowires and Co_3O_4 nanosheets, so when the current density changes greatly, the composite structure is damaged [28–30]. When the current density finally returns to 0.1 C, the discharge capacity is still up to 750 mAh/g, indicating that the rate capability of this material is excellent.

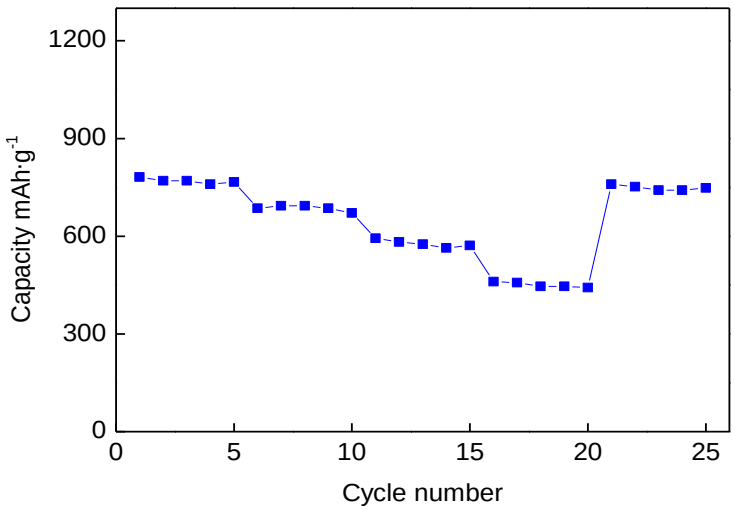

Figure 6. Rate capability curve of TiO_2/Co_3O_4 nanostructures.

3.3.3. Cyclic voltammetry test

Fig. 7 shows the cyclic voltammetry curves of the TiO_2 nanowires and the nest-like TiO_2/Co_3O_4 nanostructures after annealing at 400 °C. Fig. 7a shows the cyclic voltammetry curves of TiO_2 nanowires, and their oxidation and reduction peaks appear at 1.25 and 1.75 V, respectively, corresponding to the intercalation and de-intercalation of Li^+ in TiO_2. The integral areas of the oxidation and reduction peaks are approximately equal, indicating that the reversibility is good. The positions of the oxidation and reduction peaks correspond to the less significant discharge plateaus in Fig. 4a.

Fig. 7b shows the cyclic voltammetry curve of the nest-like TiO_2/Co_3O_4 nanostructures. Two obvious oxidation peaks appear at 0.75 and 2.2 V. After comparison with Fig. 4b, it is presumed that the 2.2 V oxidation peak corresponds to the lithium de-intercalation oxidization peak of Co_3O_4, and the 0.75 V oxidation peak corresponds to the lithium de-intercalation oxidation peak of TiO_2 [31,32]. The reduction peaks are located at 2.25 and 0.5 V. Similarly, the 2.25 V peak corresponds to the lithium intercalation reduction peak of Co_3O_4, and the 0.5 V reduction peak corresponds to the lithium intercalation reduction peak of TiO_2.

In summary, the charge and discharge capacity and battery stability of the nest-like TiO_2/Co_3O_4 nanostructures have been greatly improved. The nest-like TiO_2/Co_3O_4 nanostructure prepared through the secondary hydrothermal reaction can significantly improve the electrochemical performance of TiO_2 nanowires.

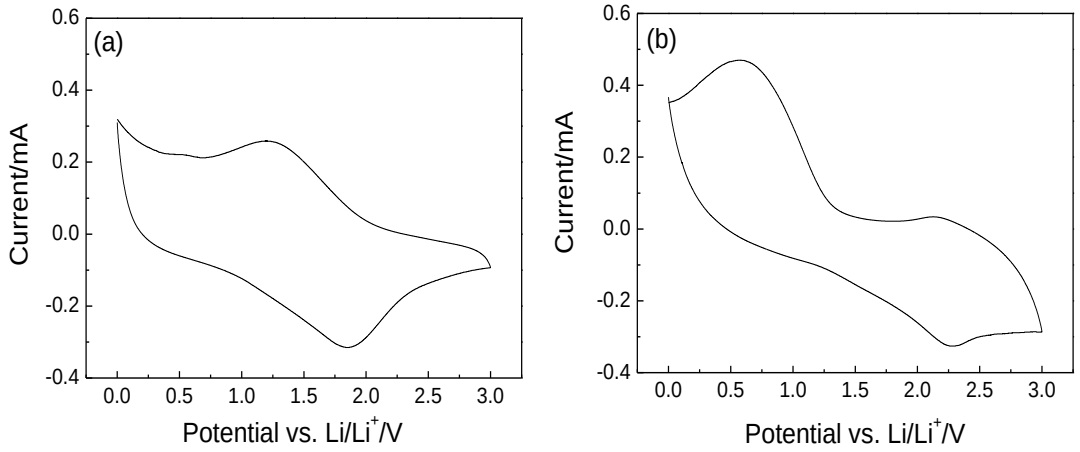

Figure 7. CV curves of (a) TiO_2 nanowires (at 180 °C for 12 h) and (b)TiO_2/Co_3O_4 nanostructures (at 180 ℃ for 12 h under an argon shield, with sintering at 400 ℃ for 5 h).

3.3.4. AC impedance test

Fig. 8 shows the AC impedance curves of the TiO_2 nanowires (Fig. 8a) and nest-like TiO_2/Co_3O_4 nanostructures (Fig. 8b) after annealing at 400 ℃, respectively. It can be seen from the figure that the impedance curves of the two nanostructures have similar characteristics, that is, the curves are composed of semicircles in the high-frequency region and oblique lines in the low-frequency region. The semicircle represents the charge transfer impedance, and the oblique line

represents the intercalation and de-intercalation of lithium ions in the electrode material [18]. Studies show that the diameter of the semicircle is proportional to the charge transfer impedance, i.e., the smaller the diameter of the semicircle is, the smaller the charge transfer impedance will be in the electrode [19]. By comparing Figs. 8a and b, we can see that the nest-like TiO_2/Co_3O_4 nanostructures are obviously smaller than the TiO_2 nanowires, which further proves that the nest-like TiO_2/Co_3O_4 nanostructures help to improve the charge conduction velocity.

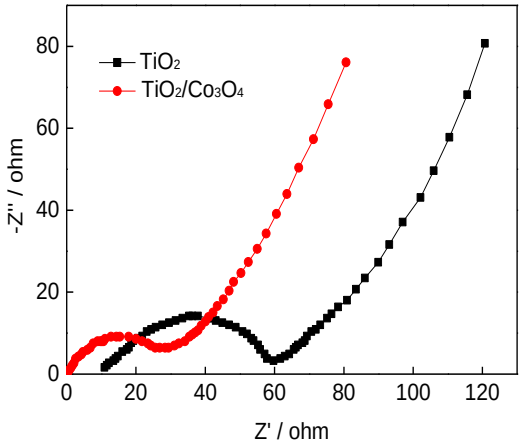

Figure 8. Electrochemical impedance spectroscopy profiles of TiO_2 nanowires (at 180 °C for 12 h) and TiO_2/Co_3O_4 nanostructures (at 180 °C for 12 h under the argon shield, with sintering at 400 °C for 5 h, a scanning voltage of 0–3 V and a scanning rate of 2 mv/s).

4. CONCLUSIONS

We have prepared a new type of nest-like TiO_2/Co_3O_4 nanostructure formed by a mechanical external force. A single nest-like TiO_2/Co_3O_4 consists of multiple flake and linear structures, with a size of ~20 μm. The nest-like nanostructure is composed of monoclinic TiO_2-B and cubic-phase Co_3O_4. The electrochemical performance test on the nest-like structure shows that at a current density of 33.5 mA/g, the first discharge capacity can be up to 777 mAh/g, and the charge capacity 759 mAh/g. After 100 cycles, the reversible capacity can still be maintained at 650 mAh/g, showing good cycling stability.

ACKNOWLEDGEMENTS
The authors are thankful for foundation support (NO 51601081 and 51665022).

References

1. J. Zhang, P. Gu, J. Xu, H. Xue, H. Pang, *Nanoscale*, 8 (2016) 18578.
2. M. Armand, J. M. Tarascon, *Nature*, 451 (2008) 652.
3. J.M. Tarascon, M. Armand. *Nature*, 414 (2001) 359.

4. S.T. Zhang, M.B. Zheng, Z.X. Lin, R. Zang, Q.L. Huang, H.G. Xue, J.M. Cao, H. Pang, *Rsc Adv.*, 6 (2016) 39925.
5. S. Liu, H. Jia, L. Han, J. Wang, P. Gao, D. Xu, J. Yang, S. Che, *Adv. Mater.*, 19 (2014) 102.
6. R. Yu, L. Zheng, P. Frédérique, A.A. Robert, G. Clare, B. Peter, *Angew. Chem. Int. Edit.*, 51 (2012) 2164.
7. S.H. Liu, Z.Y. Wang, C. Yu, H.B. Wu, G. Wang, Q. Dong, J.H. Qiu, A. Eychmüller, X Wen, *Adv. Mater.*, 25 (2013) 3462.
8. L. Hu, Q. Chen, *Nanoscale*, 6 (2014) 1236.
9. S.L. Li, Q. Xu, *Energ. Environ. Sci.*, 6 (2013) 1656.
10. J. Jiang, Y. Li, J. Liu, X. Huang, C. Yuan, X.W. Lou, *Adv. Mater.*, 24 (2012) 5166.
11. W.W. Zhou, C.W. Cheng, J.P. Liu, Y.Y Tay, J. Jiang, X.T. Jia, J. Zhang, H. Gong, H.H. Hng, T. Yu, H.J. Fan, *Adv. Funct. Mater.*, 21 (2011) 2439.
12. G.R. Wang, Y.S. Meng, L. Wang, J. Xia, F.L. Zhu, Y. Zhang, *Int. J. Electrochem. Sci.*, 12 (2017) 2618.
13. J.Y. Wang, N.L. Yang, H.J. Tang, Z.H. Dong, Q. Jin, M. Yang, D. Kisailus, H.J. Zhao, Z.Y. Tang, D. Wang, *J. Power Sources*, 238 (2013) 165.
14. Y.P. Tang, D.Q. Wu, S. Chen, F. Zhang, J.P. Jia, X.L. Feng, *Energ. Environ. Sci*, 6 (2013) 2447.
15. K. Kravchyk, L. Protesescu, M.I. Bodnarchuk, F. Krumeich, M. Yarema, M. Walter, C. Guntlin, M.V. Kovalenko, *J. Am. Chem. Soc.*, 135 (2013) 4199.
16. W.T. Li, K. Shang, Y.M. Liu, Y.F. Zhu, R.H. Zeng, L.Z. Zhao, Y.W. Wu, L. Li, Y.H. Chu, J.H. Liang, G. Liu, *Electrochim. Acta*, 174 (2015) 85.
17. Y.N. Zhang, P. Dong, X.H. Yu, S.B. Xia, J.J. Song, R.M. Yang, H.X Liang, *Int. J. Electrochem. Sci.*, 12 (2017) 6853.
18. L. Wang, J.Zhao, S. Guo, X. He, C. Jiang, C. Wan, *Int. J. Electrochem. Sci*., 5 (2010) 1113.
19. M.M. Mohamed, B.H.M. Asghar, H.A. Muathen, *Catal. Commun.*, 28 (2012) 58.
20. W.J. Feng, Y. Cao, X. Zhao, J.T. Gang,W.X. Su, *Int. J. Electrochem. Sci.*, 12 (2017) 5199.
21. D. Liu, Z. Yang, P. Wang, F. Li, D. Wang, D. He, *Nanoscale*, 5 (2013) 1917.
22. P.Y. Keng, B.Y. Kim, I.B. Shim, R. Sahoo, P.E. Veneman, N.R. Armstrong, H. Yoo, J.E
23. Pemberton, M.M. Bull, J.J. Griebel, E.L. Ratcliff, K.G. Nebesny, J. Pyun, *Acs Nano*, 3 (2009) 3143
24. H. Göktepe, H. Şahan, Ş. Patat, *Int. J. Hydrog. Energy*, 41 (2016) 9774.
25. W. Yang, J. Liu, X. Zhang, L. Chen, Y. Zhou, Z. Zou, *Appl. Energy*, (2016).
26. H. Liao, H. Zhang, H. Hong, Z. Li, G. Qin, H. Zhu, Y. Lin, *J. Membr. Sci*, 514 (2016) 332.
27. W.C. Chueh, F. El Gabaly, J.D. Sugar, N.C. Bartelt, A.H. McDaniel, K.R. Fenton, K.R. Zavadil, T. Tyliszczak, W. Lai, K.F. McCarty, *Nano Lett*, 13 (2013) 866.
28. L. Tan, Q. Tang, X. Chen, A. Hu, W. Deng, Y. Yang, L. Xu, *Electrochimica Acta*, 137 (2014) 344.
29. D. Choi, D. Wang, V.V. Viswanathan, I.-T. Bae, W. Wang, Z. Nie, J.-G. Zhang, G.L. Graff, J. Liu, Z. Yang, T. Duong, *Electrochem. Commun*, 12 (2010) 378.
30. Y. Li, D. Fu, X. Zhang, S. Qiu, C. Qin, *J. Mater. Sci. Mater. Electron*, 27 (2016) 4417.
31. X.H. Yu, Z.L. Zhan, J. Rong, Z. Liu, L. Li, J.X. Liu, *Chem. Phys. Lett*, 600 (2014) 43.
32. X.H. Yu, Z.L. Zhan, *Nanoscale Res. Lett*, 9 (2015) 516.

© 2017 The Authors. Published by ESG (www.electrochemsci.org). This article is an open access article distributed under the terms and conditions of the Creative Commons Attribution license (http://creativecommons.org/licenses/by/4.0/).